Applicability of Viscous and Inviscid Flow Solvers to the Hypersonic REST Inlet

A. Agon[1], D. Abeynayake[1] and M. Smart[2]

[1]Defence Science and Technology Organisation
Australia

[2]Centre for Hypersonics
The University of Queensland, Queensland 4072, Australia

Abstract

This paper investigates the applicability of the quick-look inviscid CFD solver Cart3D when analysing a hypersonic REST inlet. The applicability is determined by comparing the inviscid Cart3D solution to that calculated using the full viscous solution methods in the CFD++ software package. Cart3D utilises mesh adaptation, taking the human out of the loop during the meshing process, while the CFD++ domain is manually meshed using MIME grid generator. In CFD++ the viscous effects are captured using a RANS realizable k-ε turbulence model chosen through validation studies and literature review. The captured viscous effects, such as shock boundary layer interactions, are shown to significantly affect the internal inlet flow field. This highlights that the applicability of the inviscid code is limited to the external region about the compression wedge up to the crotch. The trends in mass capture sensitivity to angle of attack and sideslip angle are consistent for both codes. A by-product of this study is the understanding of appropriate analysis methodologies that may be applied to efficiently investigate future REST inlet design iterations.

Introduction

The Rectangular to Elliptical Shape Transition (REST) inlet was first designed by Professor Michael Smart from the University of Queensland at the NASA Langley Research Centre [11] and has specific design features incorporated to overcome practical hypersonic inlet problems. As the name suggests, the REST inlet transforms from a rectangular inlet to elliptical isolator cross-section. The swept leading edges and notched cowl of the rectangular inlet allow it to be self-starting, while the use of an elliptical isolator leads to lighter, stronger high pressure sections within the engine and reduces the problems associated with hypersonic corner flows [11].

The methodology used to design the Mach 8 REST inlet [11] was modified by Professor Michael Smart under contract by the Defence Science and Technology Organisation (DSTO). While extensive experimental and CFD data for the Mach 8 inlet exist, this inlet is essentially untested.

Within any hypersonic inlet, viscous effects are dominant in the boundary layer and can have a significant effect on the hypersonic flow. A study [5] finds that Euler solutions are unable to accurately predict the location of shock waves through hypersonic inlets, nor correctly model the pressure profiles at the exit plane of the inlet. Despite this, there is no evidence to suggest that the inlet external surface pressure profile and operation could not be modelled using inviscid CFD methods.

This paper outlines the inviscid and viscous CFD analysis performed on the REST inlet by DSTO. The aim of the study is to compare pressure profiles along the inlet walls and mass flow rate profiles at the end of the isolator, the motivation being to determine the applicability of inviscid CFD solvers when designing hypersonic vehicles which incorporate REST inlets.

Geometry and Cases

The inlet surface geometry and co-ordinate system is shown in figure 1 below, with the REST inlet displayed in light grey. A compression wedge is added to the inlet, and is displayed in red. The inlet is investigated at Mach numbers 4.5, 5.5 and 6.0, at α angles of 0 and 1 degrees and β angles of -1, 0 and 1 degrees. Due to the symmetry of the vehicle in the pitch plane, only one α incidence angle case needs to be run, totalling 12 cases.
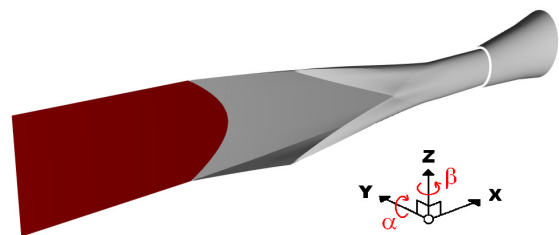
Figure 1. Inlet Co-ordinate System

Set-up of Flow Solvers and Associated Programs

The results from a NASA research code (Cart3D) are compared against those generated using the commercial viscous code (CFD++). NASA Cart3D v1.4.5 is an inviscid CFD analysis tool utilising an Euler solver. The software also takes advantage of using mostly non-body-fitted cartesian grid elements thus allowing highly efficient finite volume flow solvers to be used, resulting in fast solution times [8]. Adjoint-based adaptive mesh refinement is used to generate computationally efficient grids without requiring human in the loop interaction [1]. It offers low to medium fidelity solutions that are capable of being solved within hours.

Conversely, CFD++ offers a full numerically integrated Naiver-Stokes solution with various turbulence models and parallel computing capability. MIME (Multipurpose Intelligent Meshing Environment) is a meshing tool which can be used to generate 3D unstructured grids for complex geometries with a relatively short meshing time. However, due to the current non-mesh morphing capability of MIME all density regions in the mesh need to be manually controlled.

Cart3D's adjoint based mesh refinement feature automatically generates a grid optimised for a given adaptation functional $J(Q)$ [1]. The functional may be specified as a force coefficient or pressure values at a specified point or line sensor. A functional error for a given grid of average cell size H is obtained by comparing it to an estimated functional value on a refined grid of average cell size h, as per equation (1).

$$e = J(Q_H) - J(Q_h) \tag{1}$$

The cells which contribute most to the functional error are tagged for refinement [8], allowing the adaptation process to produce a mesh with minimum error for a particular adaptation functional. The selection of an appropriate functional is very important to allow a suitable mesh to be constructed for a given case. Two line sensors positioned in a cruciform configuration towards the end of the isolator are the selected functionals for the REST analysis.

The meshing process for CFD++ used the preliminary shock angle results produced by Cart3D to align the density boxes at the correct angles leading to decreased mesh size. Modelling of the boundary layer region is heavily dependent on the grid resolution in the near-wall region; for turbulence models to be integrated to the wall, the first computational cell above the wall must be located in the viscous sublayer. Such a mesh must have a Y+ of less than 5 [10], however, this leads to a requirement for a large number of mesh elements in the boundary layer putting a strain on computational resources. The computational resources available necessitate the use of a wall function method where the velocity profiles in the near-wall region are estimated through the use of semi-empirical relations, allowing the use of a coarser grid. The use of this method is justified by a study [7] where a wall function is able to resolve a shock-boundary layer interaction over a compression ramp at supersonic speeds, and the generated pressure profile is shown to match closely with experimental results. Wall functions are more suited when the first grid point near the wall is in the log-law region, corresponding to a Y+ of between 30 and 60 [10]. The mesh generated for the REST analysis is designed to have a Y+ also between 30 and 60 to ensure accurate results, while minimising computational cost.

Huang et al. [7] found that the realizable k-ε model, in conjunction with wall function treatment successfully resolves a shock-boundary layer interaction over a compression ramp in supersonic flow. Additionally, the realizable k-ε model is designed as a core-flow model to be used with a wall function, unlike other models such the k-ω which are designed to be integrated to the wall, and result in errors when combined with wall functions [7]. This and the computational requirement of using a wall function suggest that realizable k-ε is the most appropriate model.

A validation model testing these hypotheses was constructed to compare CFD++ results to experimental data on the Mach 8 version of the REST inlet. The study tested several turbulence models and found that the realizable k-ε model most accurately predicted the surface pressure distribution in the regions of interest.

Results

As previously mentioned, Cart3D utilises a mesh refinement process with the grid being further resolved in each adaptation cycle aiming to produce the lowest possible functional error.

Figure 2 visually demonstrates the mesh adaptation process, where the areas of interest affecting the line sensor values are being progressively resolved. By the 8th and final adaptation cycle the mesh is highly refined at the shocks, near the inlet walls, as well as most internal portions of the inlet.
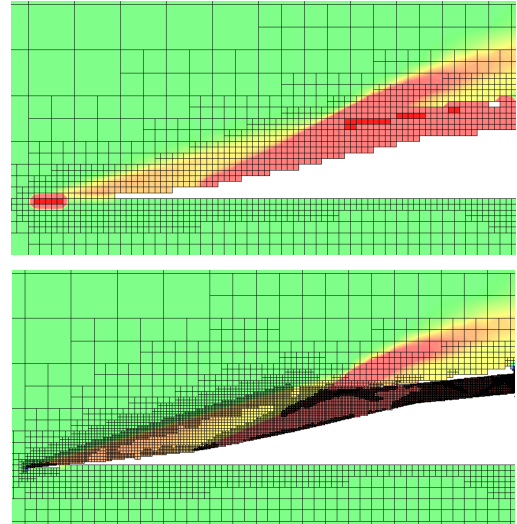
Figure 2. Progressive Mesh Adaptation Cycle 0 [top] and 8 [bottom]

Pressure contours are shown for Cart3D and CFD++ in figure 3 below. Both results indicate that the shock from the initial wedge intersects the tip of the cowl, indicating the design condition for the inlet which allows maximum mass capture [6]. The second compression shock curves up towards the tip of the cowl due to the curved surface at the body leading to an isentropic compression ramp [6].
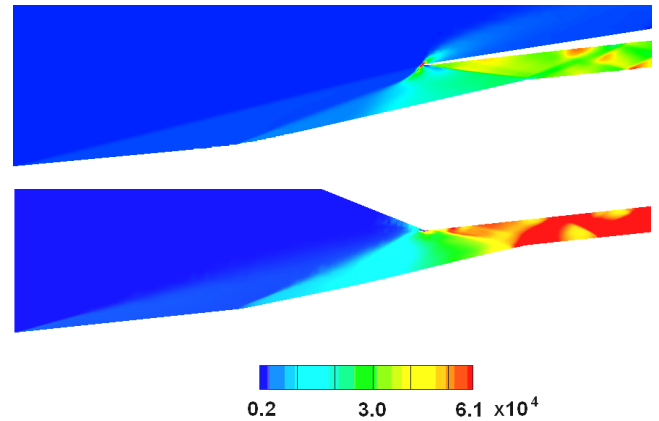
Figure 3. Cart3D [top] and CFD++ [bottom] Pressure Contours (Pascals)

The difference in the pressure contours between the two solvers is best highlighted by the difference plot shown in figure 4. It shows that the disparity in the two pressure results is mainly limited to internal areas of the inlet where differences are in the order of 4×10^4 Pa. However, external parts of the inlet show differences only in the order of 4×10^3 Pa. This highlights that the initial compression shocks are captured almost identically by both solvers.
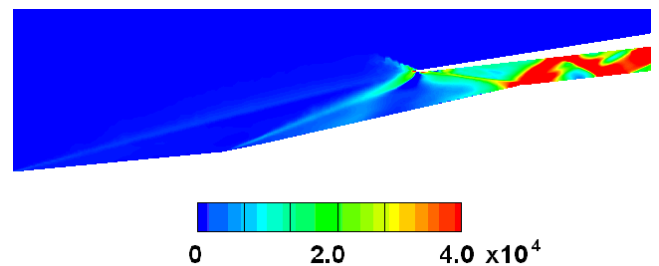
Figure 4. Data subtraction of Cart3D and CFD++ results (Pascals)

There exist several viscous phenomena that must be addressed when discussing the validity of using viscous and inviscid

solvers, these include boundary layers with adverse pressure gradients, separation/recirculation bubbles and shear layers. The locations of the incident and reflected shocks inside an inlet can be influenced by shock-boundary layer interactions (SLBI). In such phenomena, the pressure rise from the incident shock causes viscous effects such as boundary layer separations which induce a shock upstream of the impingement point, in addition to a re-attachment shock, thus significantly altering the flow field [2].

Supersonic wall bounded flow studies [3] have shown that SBLI induce large amplified wall pressure fluctuations. While these are not captured in the temporal sense by the RANS equations, they are apparent in the comparison of CFD++ and Cart3D results.

Figure 5 highlights the discrepancies between CFD++ and Cart3D surface pressure distributions, overlaid with the turbulent kinetic energy (TKE) in the viscous result. The shown pressure profiles are taken on the body side of the inlet and are non-dimensionalised by freestream pressure.

It is seen that there is good agreement prior to x = 0.4m which corresponds to the crotch region (the junction between the cowl side leading edges of the inlet). A study [4] confirms that the transitional Reynolds number is less than $6{\times}10^6$. Using this, it is estimated that the flow becomes turbulent approximately 0.1m after the initial compression wedge, well before the pressure distributions begin to diverge. This highlights that the differences in viscous and inviscid pressure distributions are unlikely due to the turbulence in the boundary layer.

The boundary layers experienced by hypersonic flight vehicles grow proportionally to the square of Mach number, and may be orders of magnitude larger than those which occur at low speeds [2]. Such thick boundary layers inside a hypersonic inlet reduce the area for the core flow, leading to increased compression ratios [9] and this is an additional reason for the surface pressures being consistently higher in the CFD++ results compared to Cart3D inside the inlet. This divergence occurs after the crotch on the body side of the inlet at the exact location of the first impinging shock. At this point, shock reflections begin to interact with the boundary layer and TKE increases, as shown in figure 5.
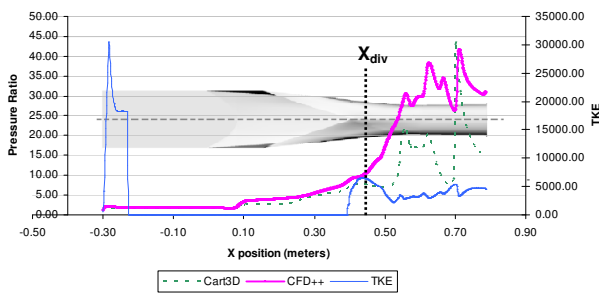
Figure 5. Mach 4.5 static pressure comparison between viscous and inviscid solvers $\alpha=0^0$, $\beta=0^0$

A constant divergence threshold was used to characterise the effect of Mach number and incidence angle on the divergence point between the viscous and inviscid results. This threshold was crossed when a difference of greater than 50% of the Cart3D value existed between the pressure profiles. This point is marked as x_{div} on figure 5 above for illustration purposes. Tables 1 to 3 show the divergence points for Mach 4.5, 5.5 and 6.0. It is observed that this point consistently occurs after an initial rise in TKE, and is located 50-100mm upstream of the point where the first shock impinges on the body side of the inlet. This agrees well with established theory, as subsonic boundary layer information flows upstream and causes an induced shock wave prior to the impingement point [2]. Clearly, x_{div} is positively correlated with freestream Mach number, as the location of the impinging shock is a function of shock angle. The shock becomes

sharper with increasing Mach number causing x_{div} to move further downstream. Furthermore, α and β incidence are seen to have minimal effect on x_{div}.

Case	x_{div}	TKE	$\Delta(P_{ratio})$	Impinging Shock
$\alpha=0^0$, $\beta=0^0$	0.45	6274	2.81	0.54
$\alpha=1^0$, $\beta=0^0$	0.46	6628	3.89	0.54
$\alpha=0^0$, $\beta=1^0$	0.46	5773	2.80	0.55

Table 1. Divergence of Pressure Results for Mach 4.5

Case	x_{div}	TKE	$\Delta(P_{ratio})$	Impinging Shock
$\alpha=0^0$, $\beta=0^0$	0.50	8320	5.81	0.57
$\alpha=1^0$, $\beta=0^0$	0.51	12500	5.72	0.57
$\alpha=0^0$, $\beta=1^0$	0.51	7900	5.64	0.57

Table 2. Divergence of Pressure Results for Mach 5.5

Case	x_{div}	TKE	$\Delta(P_{ratio})$	Impinging Shock
$\alpha=0^0$, $\beta=0^0$	0.52	9810	7.01	0.58
$\alpha=1^0$, $\beta=0^0$	0.52	9430	6.44	0.58
$\alpha=0^0$, $\beta=1^0$	0.52	9440	5.98	0.58

Table 3. Divergence of Pressure Results for Mach 6.0

Figure 6 shows the variation in the surface pressure profiles when the inlet is operated at a non-zero angle of attack. The pressure distribution remains almost identical, and this trend is consistent for both Cart3D and CFD++.
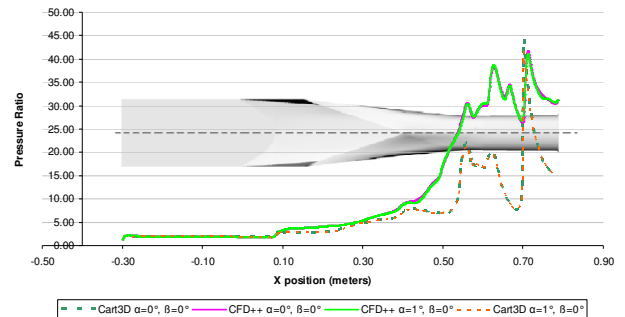
Figure 6. Mach 4.5 static pressure comparison between viscous and inviscid solvers $\alpha=0^0$, $\beta=0^0$

A similar situation is shown in Figure 7; however this time β is varied. The surface pressure distribution for both CFD++ and Cart3D are no longer identical, both codes predicting lower surface pressures when a β angle is imposed compared to the zero incidence case.
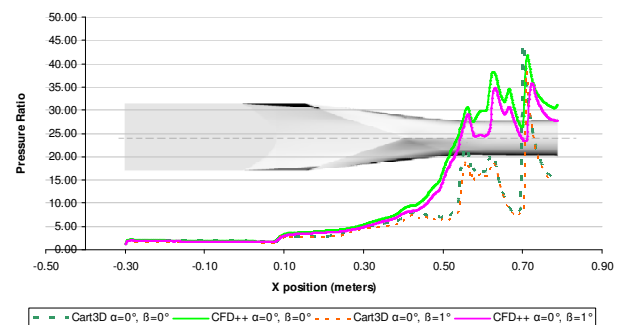
Figure 7. Mach 4.5 static pressure comparison between viscous and inviscid solvers $\alpha=0^0$, $\beta=1^0$

The sensitivity of the REST inlet to small α and β incidence at the end of the isolator may also be observed through the perspective of mass capture as shown in figure 8 below. The data highlights how both CFD++ and Cart3D predict that mass capture is more affected by increasing β incidence, rather than increasing α incidence. This highlights the engine's insensitivity to α when compared to β, and is a design feature which assists manoeuvrability when the inlet is attached to a vehicle in this orientation.
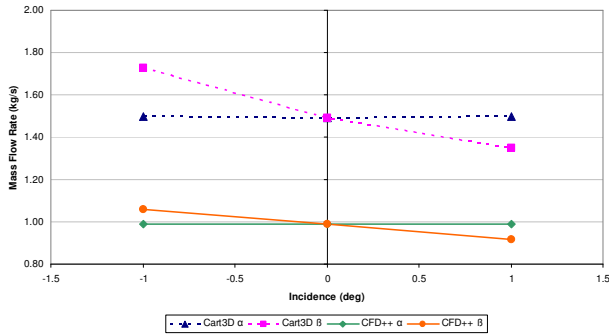
Figure 8. Mass Flow Rate at end of isolator comparison

The observed trends between the viscous and inviscid flow solvers are consistent. The Cart3D mass capture rates are consistently higher compared to the CFD++ results as viscous effects slow the flow in the internal portion of the inlet. Additionally, as explained above the boundary layer reduces the cross sectional area for the core flow, further decreasing the capture ratio. The highly swept nature of the inlet and notched cowl allows flow to spill when the leading shock is not intersecting with the cowl [11]. This highlights that the angle of the shocks, rather than viscous interactions have a greater effect on the mass capture.

Conclusions

This study shows that quick look inviscid codes such as Cart3D may be used to determine trends in mass capture such as the sensitivity to α and β angles for REST type inlets. However, viscous effects significantly affect the absolute values and would require a full physics solution to predict accurately. The rise in TKE appears to be correlated with the divergence of the data from the two CFD solvers. This divergence occurs after the crotch on the body side of the inlet, 50-100mm upstream of the first impinging shock. This implies that Cart3D may be used to determine surface pressure further downstream with larger Mach numbers. Inviscid codes are not sufficient to resolve the flow features that occur in the internal flow portion of hypersonic REST inlets. This is due to the presence of viscous effects such as large boundary layers and shock boundary layer interactions.

Acknowledgements

References

[1] Aftosmis, M.J., Melton, J.E., and Berger, M.J., Adaptive Cartesian Mesh Generation, Chapter 22 in *Handbook of Grid Generation*, Thompson, J, Weatherhill, N., and Soni, B. eds. CRC Press, 1998.

[2] Anderson, J.D., *Hypersonic and High Temperature Gas Dynamics Second Edition*, AIAA Education Series, Virginia, 2006.

[3] Baresh, S.J., Clemens, N.T. & Dolling, D.S., Relationship between upstream turbulent boundary-layer velocity fluctuations and separation shock unsteadiness. AIAA J. 40(12), 2412–2422, 2002.

[4] Laufer, J., Marte, J.E., Results and a Critical Discussion of Transition-Reynolds-Number Measurements on Insulated Cones and Flat Plates in Supersonic Wind Tunnels, NASA JPL, 1955.

[5] Cockrell, C.E., Generic Hypersonic Inlet Module Analysis, *AIAA 9th Applied Aerodynamics Conference*, 1991, 1-11.

[6] Heiser, H.H., Pratt, D.T., Hypersonic Airbreathing Propulsion, AIAA Education Series, Ohio, 1994.

[7] Huang, PG, Coakley, TJ 1993, Calculations of supersonic and hypersonic flows using compressible wall functions, *Engineering Turbulence Modelling and Experiments*, **2**, 731-738.

[8] Nemec, M. & Aftosmis, M., Adjoint Error Estimation and Adaptive Refinement for Embedded-Boundary Cartesian Meshes, in *18th AIAA Computational Fluid Dynamics Conference*, Miami, 2007, 1-16.

[9] Rowan, J.G. & Smart, M.K., Design of modular shape-transitioning inlets for a conical hypersonic vehicle, in *Proceedings of the 48th AIAA Aerospace Sciences Meeting*, USA, 2010, 1-15.

[10] Salim M., Cheah, S.C., Wall Y+ Strategy for Dealing with Wall-bounder Turbulent Flows, in *Proceedings of the International MultiConference of Engineers and Computer Scientists*, Hong Kong, , 2009, 1-6.

[11] Smart, M.K., Design of Three-Dimensional Hypersonic Inlets with Rectangular-to-Elliptical Shape Transition, *Journal of Propulsion and Power*, **15**, no. 3, 1999, 408-416.